Optical characterization of YCa4O(BO3)3 and Nd:YCa4O(BO3)3 crystals

P. Segonds, B. Boulanger, B. Menaert, Julien Zaccaro, Jean-Paul Salvestrini, M. D. Fontana, R. Moncorgé, F. Porée, G. Gadret, J. Mangin, et al.

▶ **To cite this version:**

P. Segonds, B. Boulanger, B. Menaert, Julien Zaccaro, Jean-Paul Salvestrini, et al.. Optical characterization of YCa4O(BO3)3 and Nd:YCa4O(BO3)3 crystals. Optical Materials, 2007, 29 (8), pp.975-982. ⟨10.1016/j.optmat.2005.11.036⟩. ⟨hal-00186004⟩

HAL Id: hal-00186004

https://hal.science/hal-00186004v1

Submitted on 2 Dec 2021

HAL is a multi-disciplinary open access archive for the deposit and dissemination of scientific research documents, whether they are published or not. The documents may come from teaching and research institutions in France or abroad, or from public or private research centers.

L'archive ouverte pluridisciplinaire **HAL**, est destinée au dépôt et à la diffusion de documents scientifiques de niveau recherche, publiés ou non, émanant des établissements d'enseignement et de recherche français ou étrangers, des laboratoires publics ou privés.

Distributed under a Creative Commons CC BY-NC 4.0 - Attribution - Non-commercial use - International License

Optical characterizations of $YCa_4O(BO_3)_3$ and $Nd:YCa_4O(BO_3)_3$ crystals

P. Segonds [a,*], B. Boulanger [a], B. Ménaert [b], J. Zaccaro [b], J.P. Salvestrini [c], M.D. Fontana [c], R. Moncorgé [d], F. Porée [d], G. Gadret [e], J. Mangin [e], A. Brenier [f], G. Boulon [f], G. Aka [g], D. Pelenc [h]

[a] *Laboratoire de Spectrométrie Physique, CNRS-Université Joseph Fourier, B.P. 87, 38402 St Martin d'Hères, France*
[b] *Laboratoire de Cristallographie, CNRS, Grenoble, France*
[c] *Laboratoire des Matériaux Optiques, Photonique et Systèmes, CNRS-Université de Metz, France*
[d] *Centre Interdisciplinaire de Recherches Ions Lasers, CEA-CNRS-Ecole Nationale Supérieure d'Ingénieurs-Université de Caen, France*
[e] *Laboratoire de Physique de l'Université de Bourgogne, CNRS-Université de Bourgogne, Dijon, France*
[f] *Laboratoire de Physico-chimie des Matériaux Luminescents, CNRS-Université Claude Bernard de Lyon 1, France*
[g] *Chimie Appliquée de l'Etat Solide, CNRS-Ecole Nationale Supérieure de Chimie de Paris, France*
[h] *LETI, Département Optronique, STCO, CEA-Grenoble, France*

We report a complete optical characterization of $YCa_4O(BO_3)_3$ and $Nd:YCa_4O(BO_3)_3$ crystals. We studied the relative orientation between the dielectric and the crystallographic frames as a function of the wavelength and performed accurate phase-matching angles measurements for second harmonic generation, using a single crystal cut as a sphere. We also recorded polarized luminescence spectra of Nd:YCOB along the principal axes of the dielectric frame. For both crystals, we measured the gray-tracking and the thermo-optic properties as a function of temperature and wavelength using oriented slabs. Finally, we measured all their dielectric and electro-optic coefficients, as a function of frequency and wavelength.

1. Introduction

In the past few years, literature has reported a new biaxial crystal with nonlinear optical properties belonging to the monoclinic calcium-rare-earth oxoborate family, $YCa_4O(BO_3)_3$ (YCOB), which can be doped with Nd^{3+} ions to form $Nd:YCa_4O(BO_3)_3$ (Nd:YCOB) crystals [1–3]. The simultaneous optimization of the nonlinear optical, the laser and the electro-optic properties of these crystals may lead to the achievement of Nd:YCOB compact laser sources [4]. It relies on a complete characterization of their optical properties, which is not available in literature especially for Nd:YCOB. However, it is reported in the present study.

YCOB and Nd:YCOB crystals were pulled directly from the melt, using Czochralski technique. In a first step of the optical characterization, we cut a few mm^3-volume sphere from the YCOB and Nd:YCOB boules in order to study the relative orientation between the dielectric and the crystallographic frames as a function of the wavelength. Then we cut oriented YCOB and Nd:YCOB slabs along the three principal axes of the dielectric frame and recorded polarized light transmission spectra. We also studied the color centers formation under ultra-violet (UV) and green radiations using a standard pump–probe technique. In a second step, we performed phase-matching angles measurements

* Corresponding author. Fax: +33 4 76 63 54 95.
E-mail addresses: psegonds@ujf-grenoble.fr, patricia.segonds@ujf-grenoble.fr (P. Segonds).

using the YCOB and Nd:YCOB spheres in order to determine reliable dispersion equations of the three principal refractive indices in the whole transmission domain of the crystals. These equations yield a complete description of the three-wave parametric phase-matching properties of YCOB and Nd:YCOB. We also recorded polarized light luminescence spectra using a crystal cut as a sphere in order to determine the potentiality of the laser properties of Nd:YCOB and to investigate the bi-functionality based on a simultaneous optimization of the nonlinear optical and laser properties of the crystal. In a third step, we investigated the thermo-optic coefficients as a function of temperature and wavelength, using oriented YCOB and Nd:YCOB slabs. We also studied the electro-optical and dielectric properties of YCOB and Nd:YCOB, in order to evaluate their ability to integrate other optical functions, such as electro-optic modulation.

2. Crystals growth

Due to its congruent melting, YCOB and Nd:YCOB were grown from the melt by using Czochralski technique [2,3]. We have developed a growth process for single crystals with good optical quality. The iridium crucible was 100 mm in diameter, the pulling rates were in the range of 0.5–3 mm/h and the rotation rate was chosen to keep the interface shape convex enough. Crystals were grown along the crystallographic b-axis direction. The main encountered difficulties were the fractures appearing during the cooling and the presence of inclusions in the crystal. The thermal environment had to be carefully optimized by appropriate screens in order to avoid fractures. The inclusions in the crystal were found to be linked to noise in the crystal diameter control loop, which used the crystal weight for the crucible temperature monitoring. Therefore, a particular care was taken to the quality of the mechanical translation and rotation of the pulling head on one hand and to the crystal weight measurement on the other hand, in order to reduce the noise and the resulting diameter variations. Post-growth annealing of the crystal was also required for its stabilization and for the reduction of the occurrence of fractures during the sawing. Centimetrical YCOB and 5% Nd:YCOB crystals with good optical quality were grown from the improvement of the growth process. A 5% Nd:YCOB crystal is depicted in Fig. 1.

Fig. 1. A picture of a 5% Nd:YCOB crystal, grown by using Czochralski technique. Its dimensions reach 50 mm in diameter and 120 mm in length.

3. Dielectric frame orientation as a function of the wavelength

Since YCOB crystallizes in the monoclinic crystal system, the orthonormal dielectric frame (x,y,z) does not correspond to the main axes of the crystallographic coordinate system (a,b,c): only one dielectric axis (y-axis in this case) corresponds to the crystallographic b-axis and the two other dielectric axes, x- and z-axes are in the (a,c) plane but tilted around the b-, or y-axis from the a–c ones [2]. Furthermore, the position of the x- and z-axes being not constrained by the symmetry, it may be wavelength dependent. To control that, we have implemented a new method for the study of the relative orientation between the dielectric and the crystallographic frames as a function of wavelength [5,6]. It uses a single crystal cut as a sphere, which is polished to optical quality and then is stuck on a goniometric head after X-rays orientation. This method was applied to YCOB and Nd:YCOB spheres of 5.54 mm and 7.44 mm diameter, respectively. They were stuck perpendicularly to the b-axis with a precision better than 0.05° by X-rays diffraction, using a Bruker AXS KappaCCD automatic diffractometer. They are shown in Fig. 2.

In a first step, each sphere was mounted on a X-rays automatic diffractometer which was coupled with a He–Ne laser beam. From X-rays orientation we marked out the goniometric positions of the a- and c-axes. Since it is also the x–z plane of the dielectric frame, it contains the two optical axes of internal conical refraction as shown in Fig. 3a. When a laser propagates along one of these two axes, hollow cones are easily observed, their aperture angles being enhanced by the spherical shape of the crystals [7]. From these observations we marked out the goniometric positions of the z- and x-axes. Finally, we measured $\widehat{az} = 24.7°$ and $\widehat{cx} = 13.4°$ at $\lambda = 0.6328$ μm with a precision of about ±0.1° for both YCOB and Nd:YCOB. In a second step, each sphere was successively placed at the center of an Euler circle coupled to a tuneable laser. Then, $\widehat{az}$ was measured as a function of the wavelength. The results, which were the same for both crystals, are given in Fig. 3b. It clearly appears from Fig. 3b that $\widehat{az}$ is wavelength independent for YCOB and Nd:YCOB, from the visible up to 2.2 μm, within the accuracy of ±0.5° of our measurements.

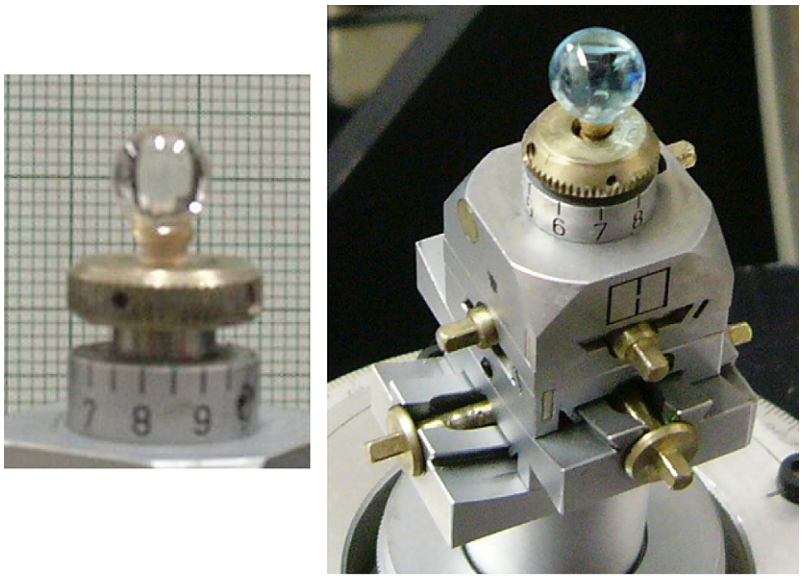

Fig. 2. Pictures of a 5.54 mm-diameter YCOB sphere (a) and of a 7.44 mm-diameter 5% Nd:YCOB sphere (b). They were stuck on a goniometric head perpendicularly to the *b*-axis.

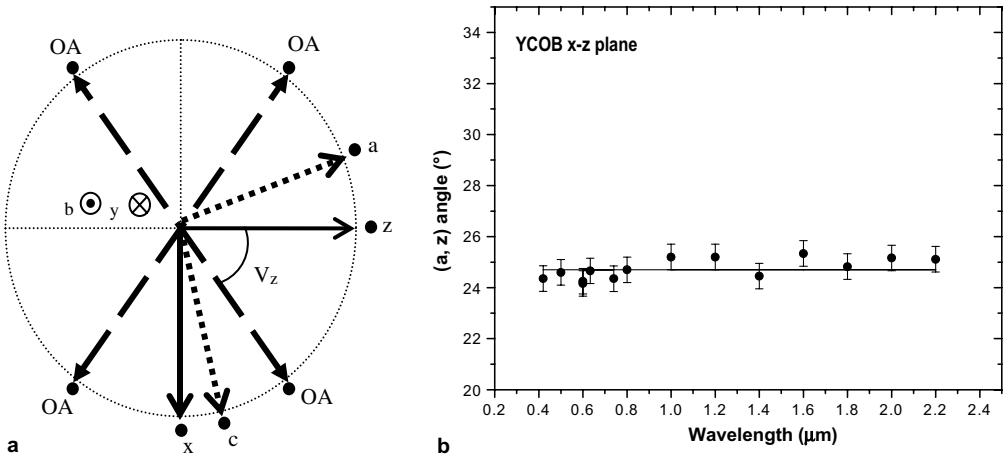

Fig. 3. Relative orientation between the crystallographic frame (a,b,c) and the dielectric frame (x,y,z) (a). V_z is the angle between the z-axis and the optical axes denoted by OA. Angle between the a- and the z-axes as a function of wavelength (b). The dot points are relative to our experimental data and the solid line is a guide for the eyes.

4. Polarized transmission spectra and study of color centers formation

From the previous orientation measurements, millimetrical YCOB and Nd:YCOB slabs were cut with their faces oriented perpendicularly to the three main axes of the dielectric frame x, y and z. A multiwire saw with free SiC abrasive was used. Polarized transmission spectra of Nd:YCOB were recorded between 0.3 μm and 3.3 μm with light polarization parallel to the x- and z-axes successively. They are given in Fig. 4, for a propagation along the y-axis of a 8 mm long slab. The spectra of Nd:YCOB show a transmission reaching 80% between 0.3 μm and 3.4 μm: the only difference compared with a YCOB unpolarized transmission spectrum given in Ref. [5], is thin absorption bands below 1 μm, due to Nd^{3+} ions doping. There are also three large infrared absorption bands peaking at 2.7 μm, 2.9 μm and 3.2 μm, which were already observed for YCOB [2,5]. Fig. 4 shows that these three absorption bands are polarization dependent, the strongest absorption occurring for light parallel to the z-axis.

Several differently oriented YCOB slabs were studied by using a standard pump–probe technique in order to determine their propensity to form color centers under high pump excitation densities around 0.532 μm and 0.266 μm. The experimental setup is shown in Fig. 5. The measurements were performed by using a frequency-doubled and -quadrupled Nd:YAG laser delivering 10-ns pulses with fluences of about 1 J/cm^2 onto samples. The probe beam was provided by a 500 ns Xe flashlamp which was synchro-

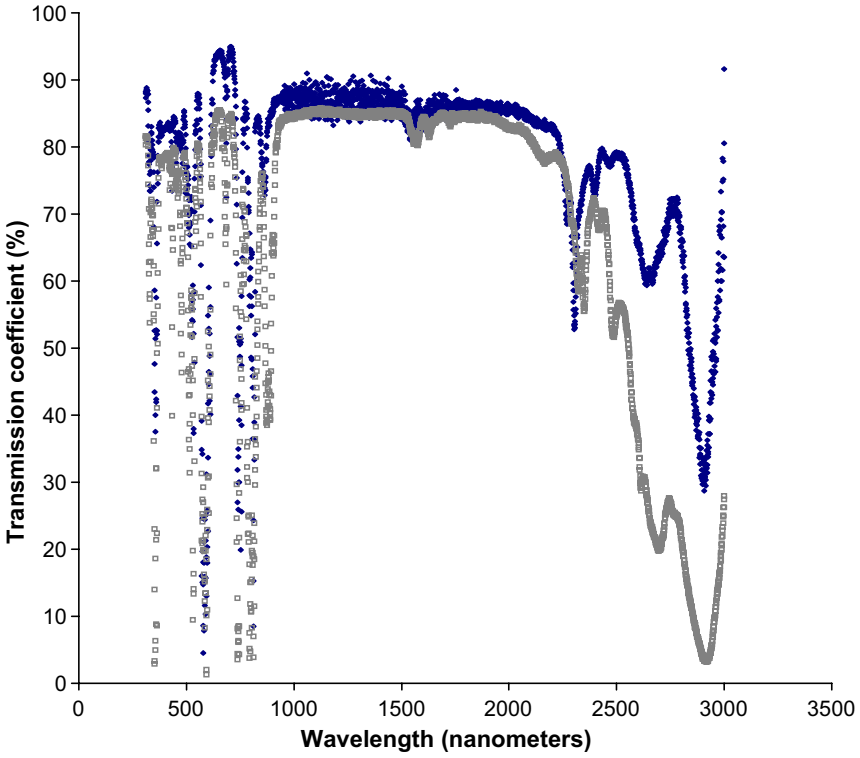

Fig. 4. Transmission spectra of Nd:YCOB using a 8 mm long oriented slab, for a propagation along the *y*-axis. The dark line corresponds to a light polarization parallel to the *x*-axis and the gray line is relative to the *z*-axis.

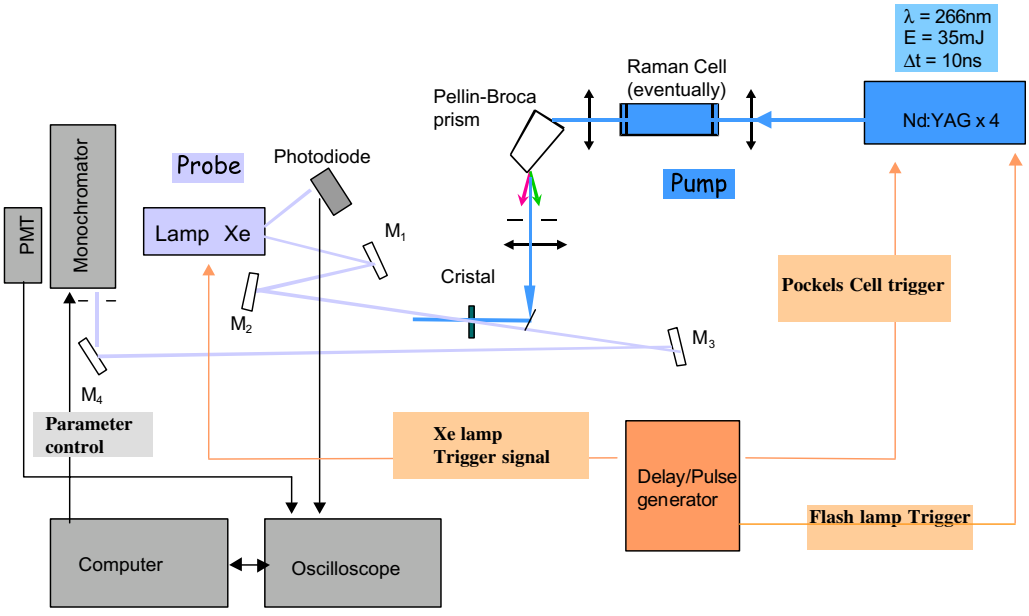

Fig. 5. Pump–probe experimental setup for the study of color centers formation of YCOB under pump excitation.

nized with the laser pulses by using a Stanford DG535 pulse generator. Transient polarized transmission spectra of the probe beam were recorded between 0.22 μm and 0.6 μm either at very short times, i.e., a few tens of nanoseconds, either at longer times, i.e., up to several minutes, after the excitation laser pulses. Whereas no transient absorption band was detected by pumping the crystals around 0.532 μm, strong and time-dependent color center absorption bands clearly appeared by using 0.266 μm pump photons. As shown in Fig. 6, two bands, which can be assigned at least to two different kinds of impurities or lattice defects, can be distinguished around 0.32 μm and 0.45 μm, the latter being predominant at the short time delays only, after the 0.266 μm excitation laser pulse. Sim-

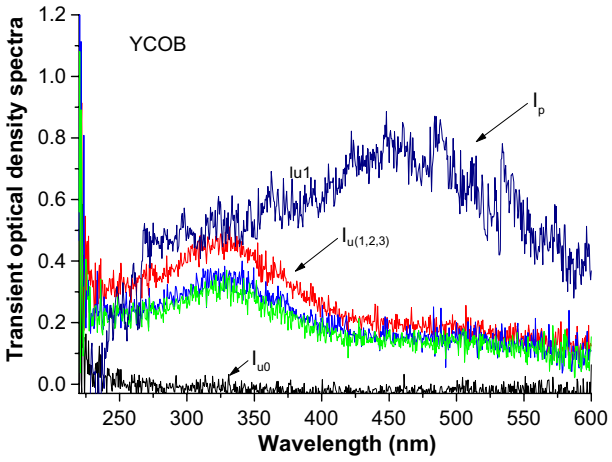

Fig. 6. Transient optical density spectra recorded in YCOB slabs before pumping (curve I_{u0}) and after 266 nm pulsed pumping at various delay-times: a few tens of nanoseconds (curve I_p) and a few minutes (curves $I_{u(1,2,3)}$) after pulsed pumping.

ilar results were obtained with other slabs cut from the same boule, under different 0.266 μm-pump and probe polarizations schemes: it revealed a pronounced gray tracking of YCOB, which decreased but not completely disappeared after several minutes exposure to the probe light of the Xe flashlamp.

5. Nonlinear optical frequency conversion and laser properties

The nonlinear optical properties study concerns second harmonic generation (SHG). We performed SHG direct phase-matching angles measurements of YCOB and Nd:YCOB as a function of the fundamental wavelength up to 3.5 μm, by using the sphere method [8]. We already used such a technique with success for the KTP arsenate isomorphous: $KTiOAsO_4$, $RbTiOAsO_4$, $CsTiOAsO_4$ [8]. An example of a measured phase-matching curve as a function of the fundamental wavelength is given in Fig. 7 for YCOB. It is relative to a type I SHG in the x–z plane. The accuracy of the measurements is of about ±0.3°. We determined reliable dispersion equations of the refractive indices by considering the phase-matching angles data as a function of the fundamental wavelength over a range as large as possible

$$n_i^2 = A_i + \frac{B_i}{\lambda^2} + \frac{C_i}{\lambda^4} - D_i\lambda^2 - E_i\lambda^4 \quad (1)$$

where i stands for x, y or z and λ is in micron [5]. We got the set of the five parameters A_i, B_i, C_i, D_i and E_i, which are listed in Table 1 from the experimental data fitting. The phase-matching angles calculated from Eq. (1) are given in Fig. 7; they are in very good agreement with experiments at any wavelength. Type I SHG phase-matching angles of Nd:YCOB were also recorded as a function of the wavelength in the x–z plane: they completely recover the data of YCOB, revealing no Nd^{3+} ions doping effect on the nonlinear optical properties.

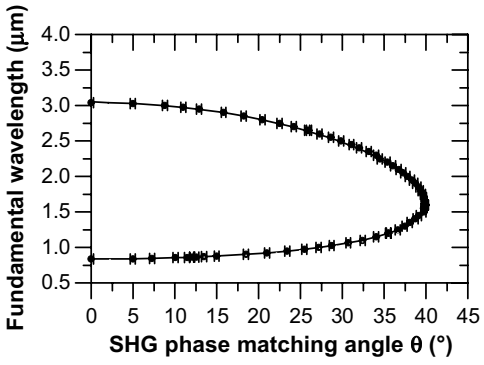

Fig. 7. Type I SHG phase-matching angles of YCOB in the x–z plane, as a function of the fundamental wavelength. The dot points are relative to our experimental data. The solid line refers to the interpolated Sellmeier equations.

Polarized luminescence spectra of Nd:YCOB were recorded around 1 μm as a function of the wavelength. It was performed for different directions of propagation in the x–z principal plane, based on the rotation of the Nd:YCOB sphere. It is to the best of our knowledge the first measurement of that kind [9]. The ability of measuring the luminescence as a function of the direction of propagation is an important issue when both the nonlinear and laser properties have to be simultaneously optimized. Considering the polarized transmission spectra of Nd:YCOB shown in Fig. 4, we selected $\lambda = 0.812$ μm as the pumping wavelength. Examples of recorded y- and z-polarized luminescence spectra of Nd:YCOB for a propagation along the x-axis are given in Fig. 8. They exhibit and a strong anisotropy and show three principal peaks, which amplitude is strongly polarization dependent: the strongest one appears at 1.060 μm, the two others around 1.070 μm and 1.090 μm. Our data are in perfect agreement with similar studies performed on 5% Nd:YCOB slabs, which validates our method [2,4]. Such measurements are in progress along other the phase-matching directions, by rotating the Nd:YCOB sphere. Especially, we study the luminescence along the 1.060 μm type I-SHG phase-matching directions for self SHG. In the future, we plan to use other directions where both the nonlinear and laser properties will be simultaneously optimized for self sum- or self difference-frequency generation.

Table 1
Fitting parameters of the dispersion equations of the principal refractive indices n_x, n_y and n_z of YCOB at room temperature

Parameters	$i = x$	$i = y$	$i = z$
A_i	2.6629	2.846	2.9027
B_i	0.034508	0.038086	0.0423
C_i	0.0009115	0.00098163	0.00068559
D_i	0.010944	0.020364	0.020262
E_i	0.000016415	0.00010088	0.00029925

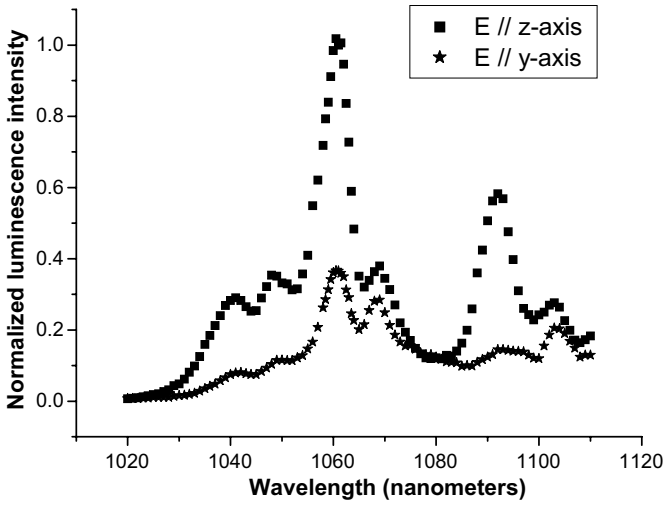

Fig. 8. Polarized luminescence spectra of Nd:YCOB for a propagation along the x-axis and with light polarized parallel to the z-axis (squares) and y-axis (stars), respectively.

6. Thermo-optical properties

We studied the temperature dependence of the normalized thermo-optical coefficients, $\beta(\lambda, T) = \frac{1}{n}\frac{dn}{dT}$, of YCOB and Nd:YCOB at several wavelengths λ. This study is of prime importance, since exposure of these crystals to high-power laser beams might lead to a phase mismatch of the nonlinear interactions due to temperature variation of the refractive indices. An interferometric method was used, running between 30 °C and 100 °C, and coupled to 0.532 μm, 0.633 μm and 1.064 μm laser sources. This technique, previously applied to the study of KTP and $LiNbO_3$, allows to determine both linear thermal expansion coefficient, $\alpha(T) = \frac{1}{L}\frac{dL}{dT}$, and normalized temperature coefficient of optical length nL, $\gamma_\lambda(T) = \frac{1}{nL}\frac{d(nL)}{dT}$. Then the normalized thermo-optic coefficients, $\beta_\lambda(T)$, can be obtained from [10]:

$$\beta_\lambda(\lambda, T) = \gamma_\lambda(\lambda, T) - \alpha(T) \quad (2)$$

The accuracy is of about of 2×10^{-7} K^{-1}. We performed measurements at 1.064 μm and 0.532 μm, on three millimetric YCOB and Nd:YCOB slabs with their optical faces cut perpendicularly to the x-, y- and z-axes. The principal linear thermal expansion coefficients, α_x, α_y and α_z of YCOB and Nd:YCOB are displayed Fig. 9 as a function of temperature, showing a linear behavior and values ranging from 3×10^{-6} to 1.3×10^{-5} K^{-1}. The corresponding linear fits given in Table 2 could suggest a difference between the thermal evolutions of the linear expansion coefficients of YCOB and Nd:YCOB. But we get from Table 2 that the difference between the values of α_x, α_y and α_z of these two crystals does not exceed 8×10^{-8} in K^{-1} units. Since this difference is within the limit of accuracy of our experiments we cannot state any significant effect of the Nd^{3+} doping.

From our measurements, we could determine the thermo-optical coefficients, β_x, β_y and β_z of YCOB and Nd:YCOB. They exhibit a linear thermal evolution and their values lie in the range 2×10^{-7}–2.8×10^{-6} K^{-1}. The corresponding interpolated thermal dependence equations are given in Table 3. It shows a weak sensitivity to temperature variations from 300 K up to 400 K, the slopes increasing slightly on going from near infrared towards

Table 2
Linear fits of the principal linear thermal expansion coefficients α as a function of the temperature T for YCOB and Nd:YCOB (measured along x-, y- and z-axes, respectively)

Linear fits (K^{-1})	YCOB	Nd:YCOB
$\alpha_x(T)$	$1.13\times10^{-8}\times T + 9.18\times10^{-6}$	$1.39\times10^{-8}\times T + 7.92\times10^{-6}$
$\alpha_y(T)$	$1.02\times10^{-8}\times T + 1.00\times10^{-6}$	$1.28\times10^{-8}\times T + 5.80\times10^{-7}$
$\alpha_z(T)$	$6.61\times10^{-9}\times T + 5.52\times10^{-6}$	$4.54\times10^{-9}\times T + 6.37\times10^{-6}$

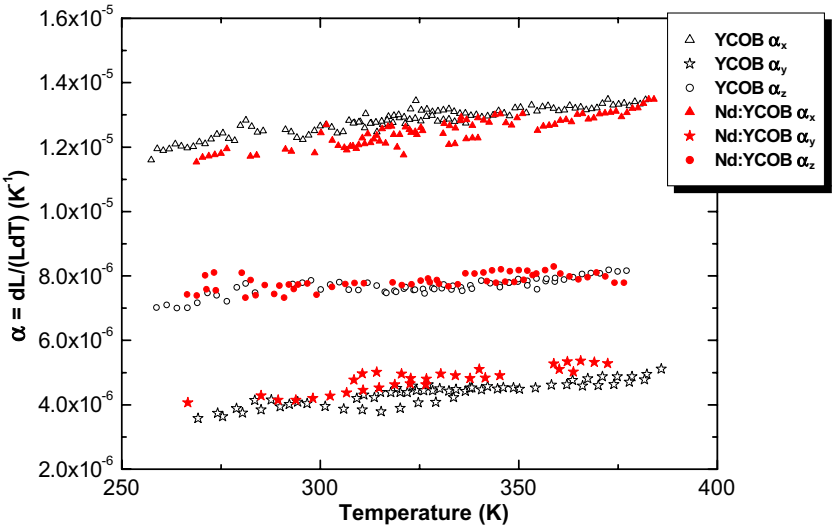

Fig. 9. Principal linear thermal expansion coefficients measured as a function of the temperature by using YCOB and Nd:YCOB oriented slabs cut along (triangles) x-, (stars) y- and (circles) z-axes.

Table 3
Linear fits of the measured principal thermo-optic coefficients β_i of YCOB and Nd:YCOB as a function of the temperature at various wavelengths

	λ (nm)	YCOB	Nd:YCOB
$\beta_x(T)$	532	$3.12\times10^{-9}\times T+4.36\times10^{-7}$	$4.78\times10^{-9}\times T-6.11\times10^{-7}$
	633	$0.66\times10^{-9}\times T+9.37\times10^{-7}$	$3.46\times10^{-9}\times T-6.64\times10^{-7}$
	1064	$2.02\times10^{-9}\times T+1.66\times10^{-8}$	$1.63\times10^{-9}\times T-2.34\times10^{-7}$
$\beta_y(T)$	532	$6.90\times10^{-9}\times T+7.97\times10^{-8}$	$7.45\times10^{-9}\times T-8.09\times10^{-7}$
	633	$2.04\times10^{-9}\times T+5.76\times10^{-7}$	$1.83\times10^{-9}\times T+4.72\times10^{-7}$
	1064	$2.04\times10^{-9}\times T+1.88\times10^{-7}$	$1.59\times10^{-9}\times T+7.30\times10^{-7}$
$\beta_z(T)$	532	$4.55\times10^{-9}\times T-6.06\times10^{-7}$	$4.50\times10^{-11}\times T+7.41\times10^{-7}$
	633	$2.38\times10^{-9}\times T-2.90\times10^{-8}$	$1.11\times10^{-9}\times T+9.53\times10^{-9}$
	1064	$3.46\times10^{-9}\times T-8.70\times10^{-7}$	$1.50\times10^{-10}\times T+8.91\times10^{-8}$
β_y–β_z at 300 K	532	14.0×10^{-7}	6.7×10^{-7}
	633	5.0×10^{-7}	6.8×10^{-7}
	1064	6.3×10^{-7}	10.7×10^{-7}

UV. The room temperature thermo-optical anisotropy, defined as β_y–β_z is also given in Table 3 at several wavelengths. If YCOB and Nd:YCOB are perfectly transparent at 1.064 μm, Nd:YCOB exhibits a strong absorption band at 0.532 μm for both y and z polarizations as shown in Fig. 4. Then it leads to a decrease of the fringes contrast obtained by using a Fabry–Perot interferometer, affecting the final accuracy of both the thermo-optic coefficients and anisotropy values. Therefore, the results given in Table 3 in terms of β_y–β_z must be checked by performing thermal acceptance measurements of the SHG at the fundamental wavelength of 1.064 μm.

7. Electro-optic and dielectric properties

The electro-optic (EO) tensor of YCOB and Nd:YCOB includes 10 nonzero independent elements. Their measurements were performed by using several YCOB and Nd:YCOB slabs with different orientations. We used the Sénarmont setup coupled to different measurements methods [11]. We considered the time response method which is able to provide the frequency dispersion of the EO coefficients [12]. It consists into the measurement of the time response of the crystal to a voltage step. For this, a large voltage pulse, up to 1 kV, is switched on the crystal. We can operate with a nanosecond rising time in order to obtain the clamped, also named as constant-strain, EO coefficients $n^3r^S_{ij}$. The measurements can also be performed in the microsecond regime for the determination of the unclamped, or constant-stress, EO coefficients $n^3r^T_{ij}$. Thus, we were able to obtain the electric field frequency dependence between 0 and 150 MHz, and the wavelength dependence in the visible and near infrared ranges of the clamped and the unclamped values of the complete set of electro-optic coefficients of YCOB and Nd:YCOB [13]. Their values, measured at 1.064 μm, are reported in Table 4. It shows that all the EO coefficients are smaller than 0.6 pm/V except for r_{53} and r_{c2}. These last EO coefficients, which involve the modulation of the refractive indices by the electric field applied along the Z-axis, are equal to 3.0 pm/V and 1.5 pm/V, respectively. We recall that the EO coefficient r^T in an unclamped crystal results from the superposition of three contributions as follows [12]: The electronic contribution r^e arises from the direct modulation of electrons by the electric field. The ionic part r^i comes from the modulation of electrons via the lattice. The acoustic contribution r^a is an indirect EO process resulting from a combination of EO and piezoelectric effects. Within the EO process, the deformation modulates the refractive index through the elasto-optic effect and thus yields the additional contribution r^a to r^T at low frequencies; $r^S=r^e+r^i$ is the true EO coefficient measured in a clamped crystal. Whereas r^a is determined from the difference between r^T and r^S, r^e can be evaluated from the nonlinear coefficient d. Both pure and Nd-doped YCOB crystals exhibit in each EO coefficient a difference r^a between the unclamped r^T and the r^S values that is not larger than 0.2 pm/V. Furthermore, the electronic part r^e is small (<1 pm/V, deduced from the value of the largest nonlinear coefficient of YCOB, which is d_{32}). Therefore, the relatively large EO coefficients r_{c2} and r_{53} originate mainly from the

Table 4
Unclamped ($n^3r^T_{ij}$) and clamped ($n^3r^S_{ij}$) electro-optic coefficients measured at 1.064 μm in YCOB and Nd:YCOB oriented slabs

Effective EO coefficient (pm/V)	YCOB	Nd:YCOB
$\lvert n_X^3 r_{a1}^T\rvert$	1.5 ± 0.15	1.9 ± 0.2
$\lvert n_X^3 r_{a2}^T\rvert$	1.3 ± 0.1	1.7 ± 0.2
$\lvert n_Z^3 r_{c1}^T\rvert$	1.1 ± 0.1	1.4 ± 0.1
$\lvert n_Z^3 r_{c2}^T\rvert$	8 ± 0.6	9 ± 0.7
$\lvert n_1^3 r_{51}^T\rvert$	2.9 ± 0.3	3.7 ± 0.3
$\lvert n_3^3 r_{53}^T\rvert$	14.1 ± 1	15.5 ± 1.1
$\lvert n_X^3 r_{a1}^S\rvert$	0.9 ± 0.1	1.2 ± 0.1
$\lvert n_X^3 r_{a2}^S\rvert$	0.9 ± 0.1	1.2 ± 0.1
$\lvert n_Z^3 r_{c1}^S\rvert$	0.6 ± 0.1	0.9 ± 0.1
$\lvert n_Z^3 r_{c2}^S\rvert$	7 ± 0.5	7.8 ± 0.6
$\lvert n_1^3 r_{51}^S\rvert$	3 ± 0.3	3.4 ± 0.3
$\lvert n_3^3 r_{53}^S\rvert$	13 ± 1	13.6 ± 1

Table 5
Unclamped (ε_{ij}^{T}) and clamped (ε_{ij}^{S}) values of the three dielectric constants measured at room temperature in YCOB and Nd:YCOB oriented slabs

Dielectric constant	YCOB	Nd:YCOB
ε_x^T	8.7 ± 0.7	9.4 ± 0.7
ε_x^S	8.5 ± 0.7	9 ± 0.7
ε_y^T	11.6 ± 0.9	11.9 ± 0.9
ε_y^S	10.7 ± 0.8	11.4 ± 0.9
ε_z^T	7.9 ± 0.6	10.1 ± 0.8
ε_z^S	7.7 ± 0.6	9.7 ± 0.8

ionic contribution. These large values can be attributed to oxygen octahedra centered on Y^{3+} and Ca^{2+} ions and linked by planar BO_3 triangles. Indeed, it is well known that oxygen octahedra have large ionic (and electronic) polarizabilities and are responsible for strong EO (and nonlinear optic) properties in oxydic crystals such as $KNbO_3$, $LiNbO_3$ or $BaTiO_3$. The EO coefficients are still larger in Nd-doped YCOB than in pure YCOB crystals, and the difference comes from the change in the ionic part that is due to Nd doping. In a simple description, r^i results from the product of the polarization-optic coefficient and the dielectric susceptibility.

Finally, to complete our set of characterizations, we performed measurements around room temperature of the frequency dependence between 1 kHz and 13 MHz of the unclamped and clamped values of the three dielectric permittivity constants of YCOB and Nd:YCOB, by using a HP impedance analyser. The corresponding data are given in Table 5. The change in dielectric permittivity ε^S that is due to Nd doping is insufficient to explain the variation in the EO coefficient r^S. Furthermore, the anisotropy in the EO properties is stronger than in the dielectric coefficient. Therefore, the enhancement of EO coefficients in Nd-doped YCOB crystal is due mainly to a change of the polarization-optic coefficient and is linked to a change in the ionic structure especially in the oxygen octahedra. As the Nd^{3+} ion has a larger radius than the Y^{3+} ion, the partial substitution of Nd^{3+} for Y^{3+} ions leads to an increase in the volume of oxygen octahedra and thus to a larger deformability, and subsequently to a larger EO coefficient.

8. Conclusion

We have reported a complete characterization of linear and nonlinear optical properties of YCOB and Nd:YCOB crystals: the orientation of the optical frame and its wavelength dependence, color centers formation under high radiation excitation, phase-matching angles measurements and luminescence spectra, the study of the thermo-optic, electro-optic and dielectric properties. Our experimental studies have shown for YCOB and Nd:YCOB a large transmission range and the same weak sensitivity to temperature for their thermo-optic properties. We also observed a pronounced gray-tracking of YCOB by using a UV pump only but it could be completely removed under light exposure. Moreover, Nd:YCOB has the same potential nonlinear optical properties for frequency conversion and the same laser properties as YCOB. Then their simultaneous optimization may lead to self-sum or self-difference generation. Finally, the values of the EO coefficients validate the potentiality of YCOB and Nd:YCOB for electro-optic modulation.

Acknowledgements

This work was undertaken within the CMDO national network "Cristaux Massifs et Dispositifs Optiques", which is supported by the French National Center of Scientific Research. CMDO network includes of the order of 20 French laboratories. The present study was performed thanks to eight of them listed at the head of this paper.

References

[1] F. Mougel, G. Aka, F. Salin, D. Pelenc, B. Ferrand, A. Kahn-Harari, D. Vivien, Adv. Solid State Lasers 26 (1999) 709.
[2] F. Mougel, Ph.D. thesis, Pierre et Marie Curie University, Paris, 1999.
[3] T. Iwai, M. Kobayashi, H. Furaya, Y. Mori, T. Sasaki, Jpn. J. Appl. Phys. 36 (1997) L276.
[4] J.M. Eichenholz, D.A. Hammons, L. Shah, Q. Ye, R.E. Peale, M. Ridcharson, B.H.T. Chai, Appl. Phys. Lett. 74 (14) (1999) 1954.
[5] P. Segonds, B. Boulanger, J.P. Fève, B. Ménaert, J. Zaccaro, G. Aka, D. Pelenc, JOSAB 21 (4) (2004) 765.
[6] B. Boulanger, P. Segonds, J.P. Fève, O. Pacaud, B. Ménaert, J. Zaccaro, Opt. Mater. 26 (2004) 464.
[7] J.P. Fève, B. Boulanger, G. Marnier, Opt. Com. 105 (1994) 243.
[8] J.P. Fève, B. Boulanger, O. Pacaud, I. Rousseau, B. Ménaert, G. Marnier, P. Villeval, C. Bonnin, G.M. Loiacono, J. Opt. Soc. Am. B 17 (5) (2000) 775.
[9] P. Segonds, B. Boulanger, B. Ménaert, J. Zaccaro, J.P. Salvestrini, M.D. Fontana, R. Moncorgé, F. Porée, G. Gadret, J. Mangin, G. Aka, D. Pelenc, in: Proceedings of 14th International Conference on Crystal Growth (ICCG'14), Grenoble, August 2004.
[10] J. Mangin, P. Strimer, L. Lahlou-Kassi, Meas. Sci. Technol. 4 (1993) 826.
[11] M. Aillerie, N. Theofanous, M.D. Fontana, Appl. Phys. B 70 (2000) 317.
[12] M. Abarkan, J.P. Salvestrini, M. Aillerie, M.D. Fontana, Appl. Opt. 42 (13) (2003) 2346.
[13] M. Abarkan, J.P. Salvestrini, D. Pelenc, M.D. Fontana, JOSAB 22 (2) (2005) 398.